Thermal Debinding and Sintering of water atomised SS316L Metal Injection Moulding Process

A M Amin[1], M H I Ibrahim[1], R Asmawi[1], N Mustaffa[1], M Y Hashim

[1]Advanced Materials and Manufacturing Centre, Universiti Tun Hussein Onn Malaysia, 86400 Parit Raja, Batu Pahat, Johor, MalaysiaType the corresponding

Corresponding author: azriszul@uthm.edu.my, mdhalim@uthm.edu.my, roslias@uthm.edu.my, nj.wawa@gmail.com, yusni@uthm.edu.my

Abstract. Thermal debinding of SS316L metal injection moulding samples was done with temperatures of 400ºC, 500ºC and 600ºC was done. Weight loss, density and shrinkage values of the brown part being analysed. X-ray diffraction (XRD) and scanning electron microscopy (SEM)/electron dispersive spectroscopy (EDS) were used to monitor the carburization and oxidation of the thermal debound samples. It is found that, samples under thermal debound temperature of 400ºC was less oxidation and carburising as compare to other temperature. Weight loss also indicates higher in percentage although the percentage shrinkage is less. XRD pattern also indicates minor affected in peaks changes as compare to other temperature. Sintering of the thermal debound samples of 400ºC temperature shows good microstructure formation and mechanical properties.

1. Introduction

Metal injection molding is a manufacturing process with a capability of producing complex geometry and intricate parts from mixing of metals, ceramic or cermet powder with combination of polymers, wax and surfactant[1] with a few shot as compare to other fabrication process[2]–[4]. Due to its versatility, near net shape and less materials waste, it's becomes attraction to most researchers in exploiting it into new dimensions whether in terms of its binder, powder characteristic, injection molding conditions, debinding and sintering[5].

Typically, a multi-component binder system is used for obtaining a low viscosity melt during injection molding for shape replication and retaining part shape during debinding. Feedstock, produced by mixing a temporary binder system and metal powder, is forced into a mold cavity during injection molding to adopt the shape of the cavity. After that, the binder system is removed during debinding, leaving a porous, fragile debound part which was subsequently densified during sintering. Among the four processing steps, debinding is the most time consuming. A successful debinding without introducing deformation and defects such as cracks are important for MIM since defects cannot be rectified in subsequent sintering step[6].

Debinding is a crucial problem with MIM because the time for binder removal depends on the part thickness. Consequently, several manufactures have set upper limits on section thickness ranging from 10 to 50mm[7], [8]. Depending on the type of the binder used, there are several debinding techniques, categorized as solvent, thermal and catalytic processes. Often, the lower molecular weight binder component is dissolved into a fluid in a process termed “solvent debinding”[9]. During solvent

debinding process, effect of solvent to feed ratio, temperature, types of solvent influenced the weight loss and diffusivity coefficient of the removing waxes from the green compacts[8]. Geometry of the solvent debound parts also influence the time consuming of waxes removal from the green compact[10]. Therefore, the goal in debinding is to remove the binder in the shortest time with the least impact on the compact.

Thermal debinding process is the process of removing backbone polymer from the brown compact (after solvent debinding process). Removing of the backbone polymers required several hundred degrees of temperature and usually base on thermogravimetric analysis (TGA) of the polymer. It is a crucial process since incomplete removal of polymer could affects the mechanical properties of the sintered parts since carbon residue could interact with the metal base and producing carbide precipitation. Heating rates, thermal atmosphere and temperatures of the thermal debinding process is important since it could affect the oxidation behavior of the part surface and increasing the parts defects before sintering process[6], [11].

In this paper, 316 L stainless steel molded parts were debound via two stage debinding which were solvent and thermal under air atmosphere before undergo sintering process using high vacuum furnace. Effect of thermal debinding and sintering on weight loss, shrinkage value and density were determined. Mechanical properties and morphology of the thermal and sintered part also being analysed.

2. Experimental work

The 316L water atomized stainless steel powder used in this study has mean particle size of 6μm. Particles size was measured via particle analyser Fritsch analysette 22 compact. The stainless steel powder has the tap density of 8.0471 g/cm^3 and was supplied by Epson Atmix Japan. Figure 1 shows the powder particles size distribution and powder morphology of the 316L water atomized stainless steel. Physical properties and the chemical composition of the powders is shown in Table 1.

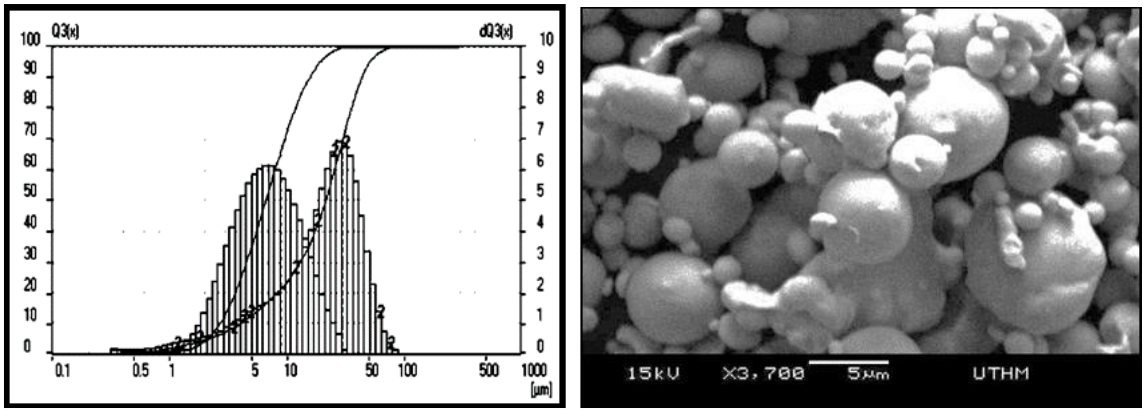

(a) (b)

Figure 1: (a) Particle size distribution and (b) SEM image of water atomised 316L stainless steel powder (PF-10F)

Table 1: Physical properties and chemical composition of 316L stainless steel metal powder

Powder size and density

Powder SS316L Epson Atmix Corp	Size	D10	D50	D90	Density
	6.0μm	2.87μm	5.96μm	10.65μm	8.0471 g/cm^3

Powder chemical composition (% wt)

Ci	Si	Mn	P	S	Ni	Cr	Mo	Cu
0.027	0.84	0.19	0.016	0.012	12.20	16.40	2.10	0.03

Table 2: Binder composition and thermal properties of binder components

Binder	**Fraction in binder**	**Density (gcm^{-3})**	**Melting Temperature (^{o}C)**	**Degradation Range (^{o}C)**
Polypropylene (PP)	**0.5 (6.9g)**	**0.90**	**165**	**350~470**
RWL derivatives	**0.5 (6.9g)**	**0.90**	**50**	**270~360**

For making the feedstock, 316L stainless steel powder of 60% powder volume which is equivalent to 186.1g of powder weight along with binder composition shown in Table. 2 was used. 60% powder loading was chosen because it is approximately 5% below the critical powder volume concentration[12] which in this case Critical Powder Volume Concentration (CPVC) of the selected stainless steel powder was found to be 64.8%[13]. The compound was blended using Brabender Plastograph EC mixer at temperature of 175°C with 30rpm for 90min. The compound were left cool at the ambient atmosphere and being crushed into smaller pallets. The feedstock then being tested with TA instruments of Differential Scanning Calorimeter (DSC) (Figure 2(a)) under nitrogen atmosphere with flow rate 50ml/min and heating rate of 5^{o}C/min. Compatibility between binder components and the behavior of the melting peak were determined before and after the blending process[14]. Thermogravimetric analysis (TGA) (Figure 2(b)) were performed under air atmosphere using TG-DTA Linseis to monitor the degradation temperature of binder components. The heating rate of thermal debinding could also be established base on feedstock and neat binder constituents.

After blending process was done, the feedstock were injected using horizontal injection moulding machine to obtain the green sample as shown in Figure 2(a). Optimization of the green density and strength was done during injection molding process (will not be discussed in this paper). RWL binder constituents then being removed via solvent extraction or debinding by immersing green samples in hexane at temperature of 60^{o}C for 3 hours using memert solvent bath (Figure 2(b))[15]. Samples were left dried under ambient atmosphere for a day in making sure that the solvent entrapped inside the brown sample will be dried out. Figure 2(c) shows the comparison of green and brown part after solvent extraction process.

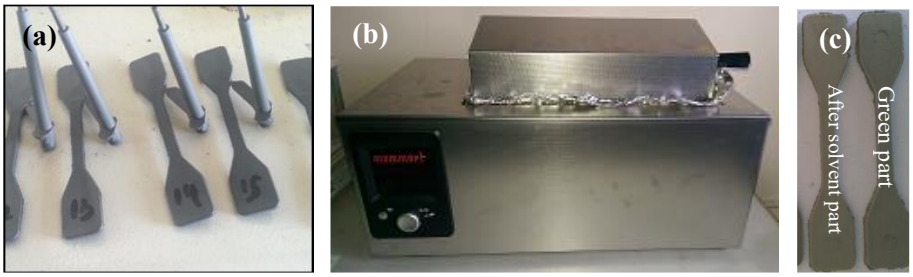

Figure 2: (a) Injected green samples, (b) solvent bath for solvent extraction and (c) comparison of green and brown sample after solvent extraction

Thermal debinding was done in removing PP out from the brown compact using Protherm high temperature furnace with heating rates of 10, 20 and 30^{o}C/min. Thermal degradation temperatures were left varies at 400^{o}C, 500^{o}C and 600^{o}C with dwell time of 100 min. After being thermally debound, the samples were left cool by furnace cool before taken out for sintering process. Sintering was done under high vacuum furnace with heating rates of 5^{o}C/min with pressure of 10^{-2}mbar or 1 Torr[16] and left cool by furnace cool. Temperature used for sintering was selected at 1360^{o}C with dwell time of 100min[17].

The dimensions, density and weight of the samples after solvent, thermal and sintered specimens were measured to calculate the effect of each process on shrinkage and density properties with respect to green samples. Tensile properties of the sintered samples were determined using GOTECH Tensile Automated Materials Testing System. The yield strength, ultimate strength and elongation were measured at speed of 5 mm/min.

The scanning electron microscopy (SEM) and energy dispersive spectroscopy (EDS) photographs of the binder system and cavities created in the green parts before, after solvent extraction and thermal debinding were monitored. XRD analysis of brown part after thermal debinding also being done for monitoring the oxidation, carbonization and carburization. The microstructure analysis also was carried out using optical microscopy, SEM/EDS and XRD pattern of the sintered part.

3. Results and discussion

In this section, thermal characteristic of binder components for the feedstock were discussed. Effect of temperature and heating rate on properties of shrinkage and weight loss of the samples after thermal debinding process were discussed. Surface morphology, oxidation and carbonization/carburization of the thermal debound samples were monitored and analysed via SEM/EDS and XRD. Mechanical properties of the sintered samples were also being discussed.

3.1. Characteristics of binder components for feedstock binder formulation

Figure 3 represents DSC heating curves graphically for RWL, PP and feedstock. For feedstock, there are two temperature peaks in endothermic side which is solid-liquid transition of PP and RWL. The solid–liquid transition temperature represents the melting point of the material. The first one was caused by RWL and the second peak due to PP. These temperatures are slightly lower than the melting points of those binders measured independently as indicated in Figure 3. These differences is called melting points of depression which results from the blended of RWL, PP and SS316L powder[14]. This indicates that all two components of binder interacted to a certain degree but did not completely dissolve into each other[18]. The heat of fusion of PP shows the larger values as compare to RWL. This suggest that PP takes more time to cool to room temperature and indicating that PP is a good backbone binder since larger heat of fusion could avoid the molded sample under high thermal stresses due to quick freezing of lower heat of fusion[18]. The binder components on the feedstock seems compatible since the different melting temperatures of the binder systems ensure that when one binder

component (wax) has melted, the remaining binder component (polymer) act as backbone support, retaining the shape of the molded part[8], [19], [20].

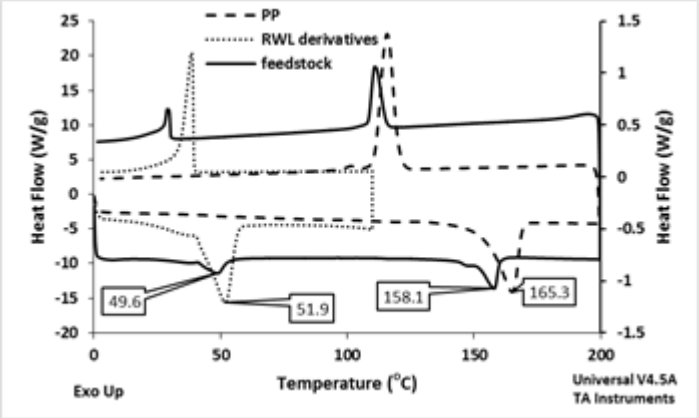

Figure 3: DSC curves of RWL derivatives, PP and feedstock

TGA analysis was done to gain an information of the decomposition temperature of the binder constituents and also to establish the heating rate and temperature of thermal debinding process[14], [19]. Figure 4 shows the TGA profile of degradation temperature of binder components and binder constituents in feedstock. Heating rate used was 10ºC/min. It can be seen that the degradation of binder components are in the range of 200ºC-600ºC and 250ºC-460ºC for RWL and PP respectively which indicates that RWL has the lower thermal stability than the PP. Thus, the mixing temperature was set higher than the highest melting point (165ºC for PP), but lower than the lowest degradation temperature of the binder components (200ºC for RWL). Consequently, the suitable mixing temperatures for formulating the binder system was chosen to be 175ºC.

TGA analysis of the brown samples was done after performing thermal debound process to monitor the remaining RWL and PP inside the brown compact as shown in Figure 4. It can be seen that the brown part after thermal process of 400ºC with heating rate of 10ºC/min shown no further degradation profile of any binder constituent which indicates that the binder was successfully removed via thermal pyrolysis.

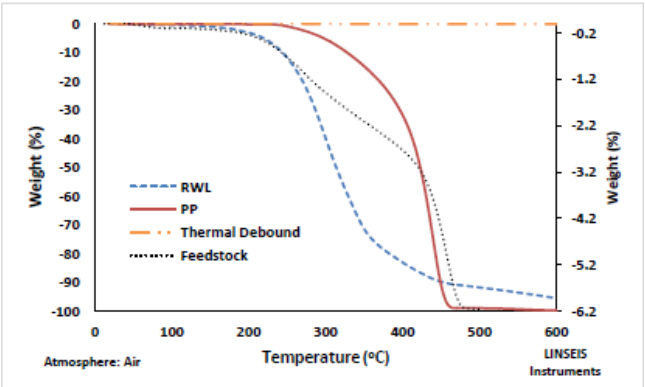

Figure 4: TGA profile of the binder constituents and after thermal debinding process

3.2. Shrinkage length of thermal debound part

Length of the thermal debound samples under the temperature of 600ºC and 500ºC with heating rate 20ºC/min were measured for shrinkage using vernier calliper. 5 samples were measured for each temperature. It is found that the length of sample under 600ºC temperature was increased by 0.53% as compare to 500ºC temperature which were shrink for 0.9%. The increased in length was not due to incomplete binder removal since binder is completely burn out at temperature of 600ºC as shown in Figure 4. The increase in length was due to the oxidation level of the samples and this was best explained by L. Liu et al. [6]. This can be seen in Figure 5(a) where samples under 600ºC temperature has higher length than the 500ºC temperature. Figure 5(c) shows the comparison of samples under 600ºC and 500ºC temperature with samples after solvent debound. The samples of 600ºC has no significant shrinkage with respect to after solvent debound sample where else 500ºC samples shows part shrinkage.

Samples under 400ºC thermal debinding also shows part shrinkage as compare to green and after solvent debinding process (Figure 5(b). The visual results shows that binder removal also occurs at temperature of 400ºC and this is proved by the TGA results (Figure 4) where the optimum degradation temperature of the PP (high slope) is at approximately 400ºC.

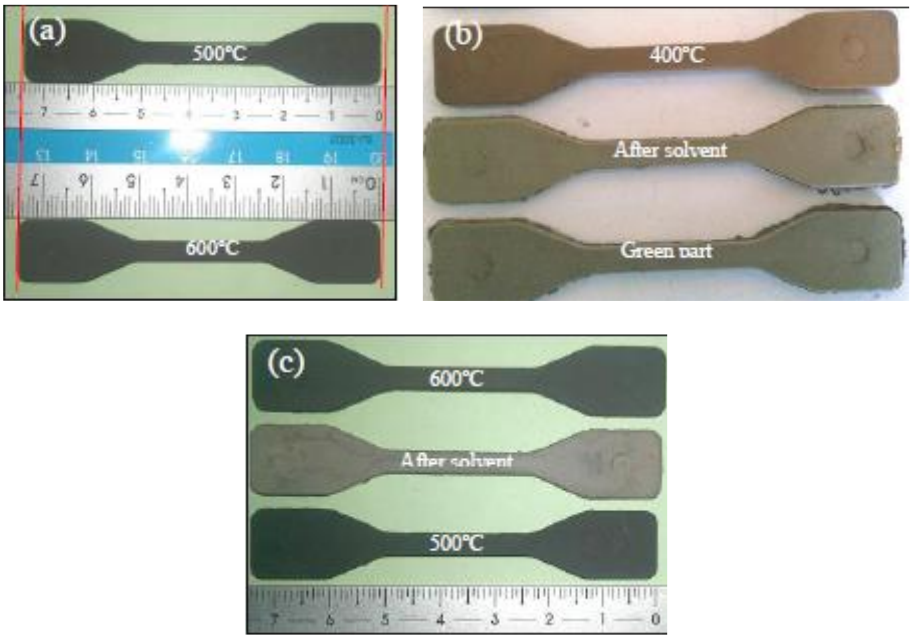

Figure 5: Visual examination of part samples under thermal debinding with different temperature

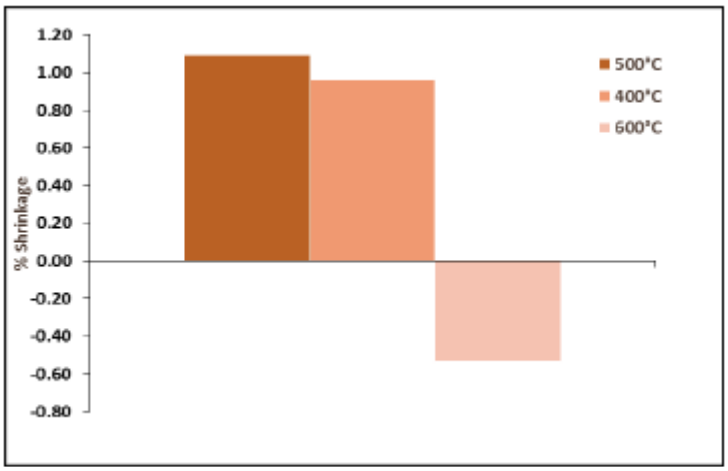

Figure 6: % shrinkage of samples at different temperature relatives to green samples

From the Figure 6, samples under thermal debound of 500ºC shows the higher values of shrinkage which indicates that most of the binder being decompose which allows the metal powder particles closely packing toward each other[21].

3.3. Weight loss of thermal debound samples.

In this section, weight loss of the samples under 400ºC temperature being compared with 500ºC temperature. From the data shown in Figure 7, samples under 400ºC temperature shows the higher weight removal as compare to 500ºC temperature. Shrinkage values of samples under 500ºC temperature was higher due to effective removal of binder and this was proved in Figure 4. Although at this temperatures complete removal of binder occurred, the weight loss was less as compared to samples under 400ºC temperature, which explained that some oxide formation on the surface of metal powder particles contribute to decrease the weight loss of the samples [22]. This was explained by Klar and Samal [23] where as a results of high temperature during the thermal debinding process, the carbon residue was decrease but increase in oxidation level under the air atmosphere of thermal debinding. As compare to samples under 400ºC temperature, the formation of the metal oxidation is low which results in increasing the percentage weight loss of the samples [6]. Carbon residue did not gave much influence on the weight loss most probably due to carbon residue from oxidative degradation of binder was forming to gaseous products at this temperature [22].

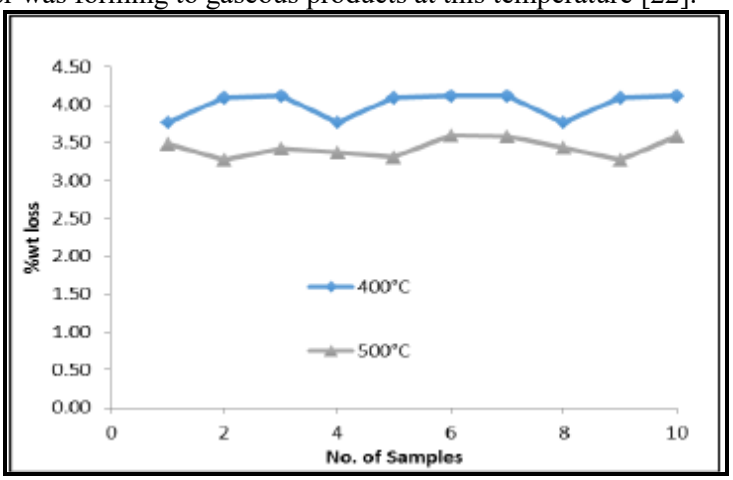

Figure 7: % weight loss of the samples between under thermal debound of 400ºC and 500ºC temperature relative to solvent samples

3.4. XRD and SEM/EDS analysis of thermal debound samples.

Analysis of the thermal debound samples was continued with XRD pattern and being compared with raw stainless steel 316L powder (Figure 8). As can be seen in the Figure 8, as-received powder has a dual-phase structure consisting of γ-austenite (faced centred cubic) peaks and β-martensitic (body centred cubic) peaks [24]. The austenite phase appears to be the predominant phase in the as-received powder. Small amounts of carbon usually being added to the stainless steel of powder where this carbon atoms will react with the oxygen during sintering and produce gaseous product and reduce the oxidation level [23]. As can be seen this carbon was interstitial diffuse in the matrix, resulting in distortion of the matrix and produce β-martensitic phases.

Samples under 600ºC temperature shows oxidation peaks as indicated in Figure 8. These peaks was emerge as the γ-austenite and β-martensitic phase decrease. The oxidation was confirmed with the SEM/EDS analysis shown in Figure 9. The oxygen element percentage shown in the EDS spot analysis is higher which strongly indicates oxidation occurs on the compact powder samples under 600ºC temperature. This oxidation was due to ferum oxide (Fe_2O_3) and chromium oxide (Cr_2O_3) formation on the powder particles[25], [26].

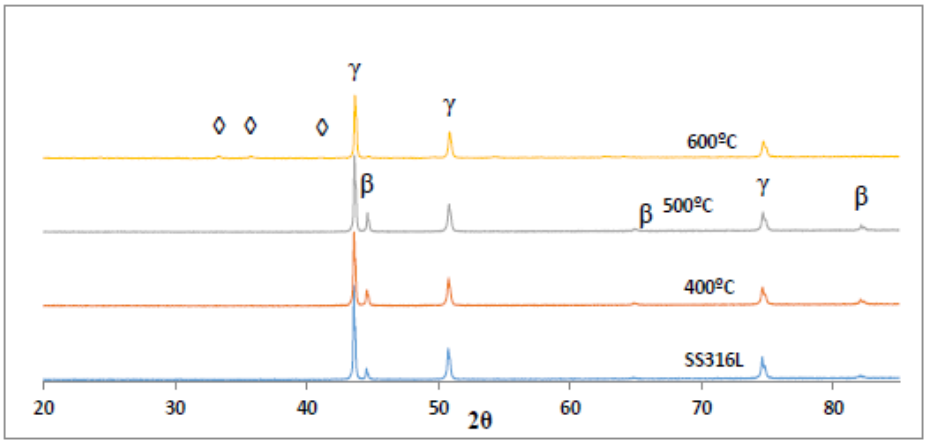

Figure 8: Comparison of the XRD pattern of the samples under different thermal debinding temperature and raw SS316L powder (◊ = Ferum Oxide (Fe_2O_3) and Chromium Oxide (Cr_2O_3), γ-Austenite phase, β-martensitic phase)

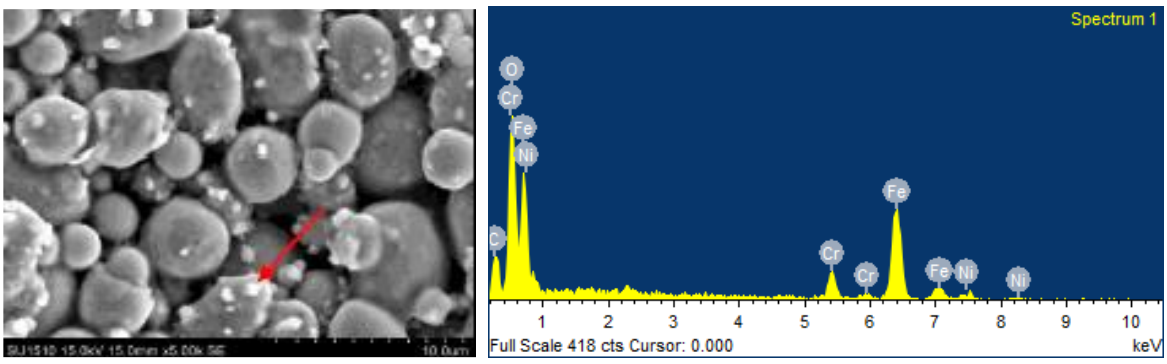

Figure 9: SEM microstructure of the samples under 600ºC thermal debinding and EDS spot analysis on the red arrow area

XRD pattern from Figure 8 was magnified in the region between 40 theta and 50 theta for 500ºC and 400ºC temperature shown in Figure 10. It can be seen that for samples under 500ºC temperature, small increment of the β- martensitic phase was detected as compared to as-received SS316L powder which was due to the carbon residue resulting from the high decomposition of binder. The excess in carbon results in interstitial diffusion of carbon atom and distort the structure of the γ-austenite phases and become increase in β-martensitic phases[23]. This can be seen with the decrease in intensity of the γ-austenite phase and increase in intensity for β-martensitic phase as compare to raw 316L powder. This interstitial diffusion of carbon atom also has slight influence in lower weight loss of samples part under this temperature. Further analysis using SEM/EDS was done using EDS spot analysis which indicates that the carbon elements was low as compare to oxygen elements. The amount of Fe in existence with Oxygen is higher as shown in Figure 11[27]. The peaks at the lower keV energy shows that the oxide elements has almost the same peaks of ferum element at the higher keV energy. Thus indicates that oxide formation occurs at this temperature.

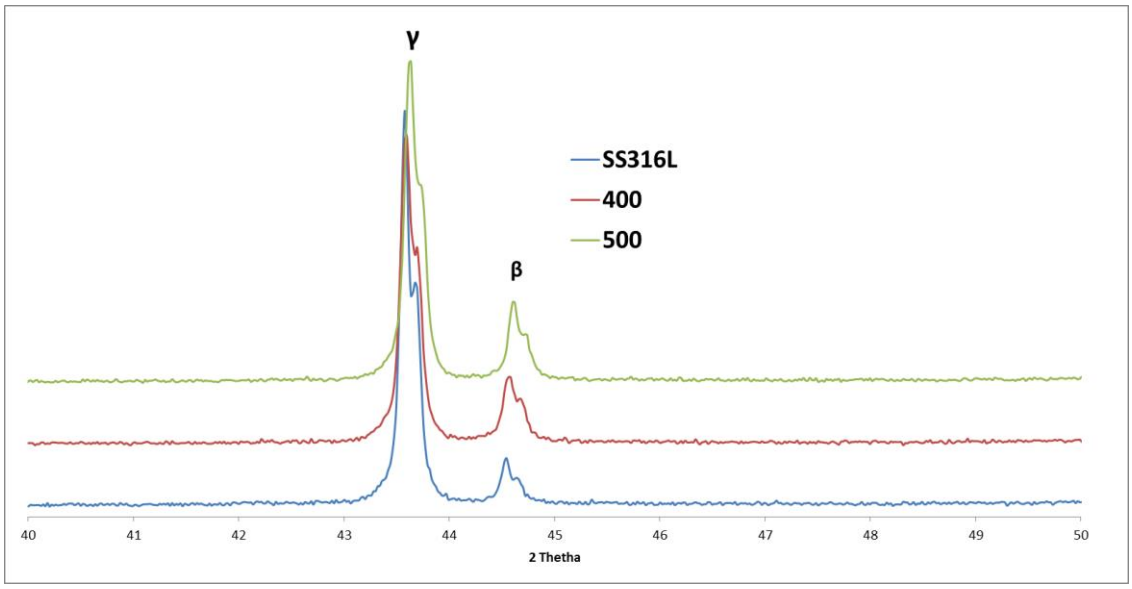

Figure 10: Comparison of decrease in austenite and increase in martensitic XRD pattern under different thermal debinding samples relatives to raw SS316L powder

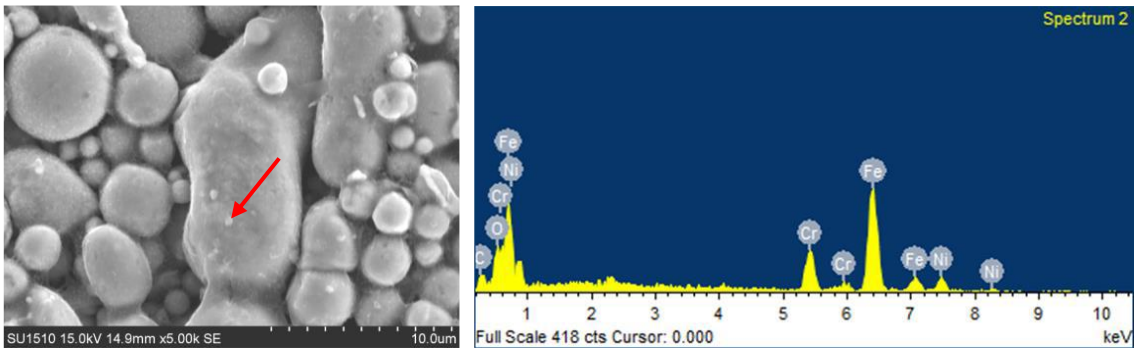

Figure 11: SEM microstructure of the samples under 500ºC thermal debinding and EDS spot analysis on the red arrow area

For samples that undergo 400ºC thermal debound, the XRD pattern shows little increase in β-martensitic peak as compare to 500ºC sample. The existence of ferum element with oxygen is much lower than the 500ºC samples. However, the carbon element was higher which due to some of the PP was not fully decompose at this temperature and producing high peak in carbon element as shown Figure 12. This assumption seems possible since carbon residue is much lower to diffuse interstitially into the γ-austenite matrix and producing β-martensitic structure. this conditions has been explain in detail by E. Klar and P. Samal[23] whereas the temperature of the thermal debound process increase in air atmosphere, the carbon residue will decrease and oxidation become increase. The color of the samples under different debinding temperature also shows different color on its surface. Parts under 500ºC temperature has brown black surface color as compare to 400ºC samples which is brown in color[28]. The black surface indicates strong carburization of the parts as compare to brown part which results from carbonization of the decomposition of the binder constituents. From this results, temperature of 400ºC were used for removing PP from the samples.

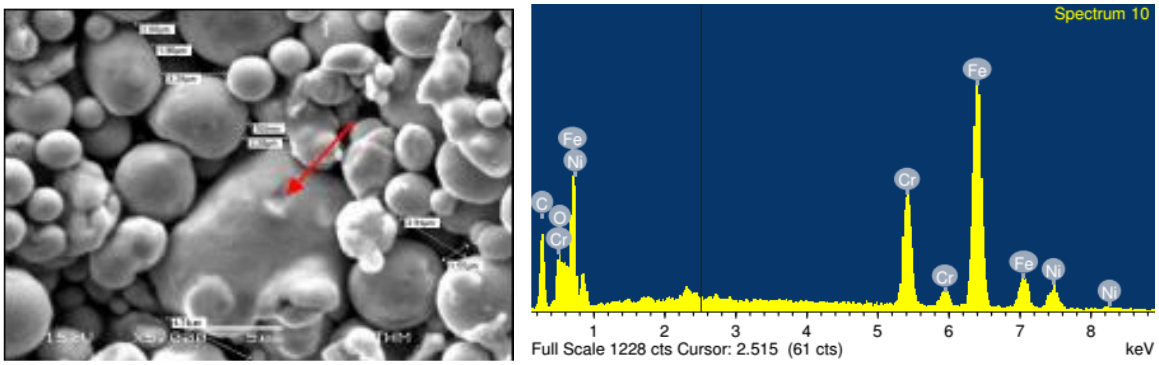

Figure 12: SEM microstructure of the samples under 400ºC thermal debinding and EDS spot analysis on the red arrow area

3.5. Sintering under high vacuum furnace

From Figure 13, shrinkage length values of the samples after sintering process increase drastically which is by 14.45% as compare to the green samples which resulted in increased in density by 97% (Figure 14). This was due to most of the binder were burn off and powder particles were coalesce and closely pack as compare to samples under thermal debinding where the particles closely pack together without any joining phase transformation. This also indicates that most of the carbon residues was diffuse out of the samples.

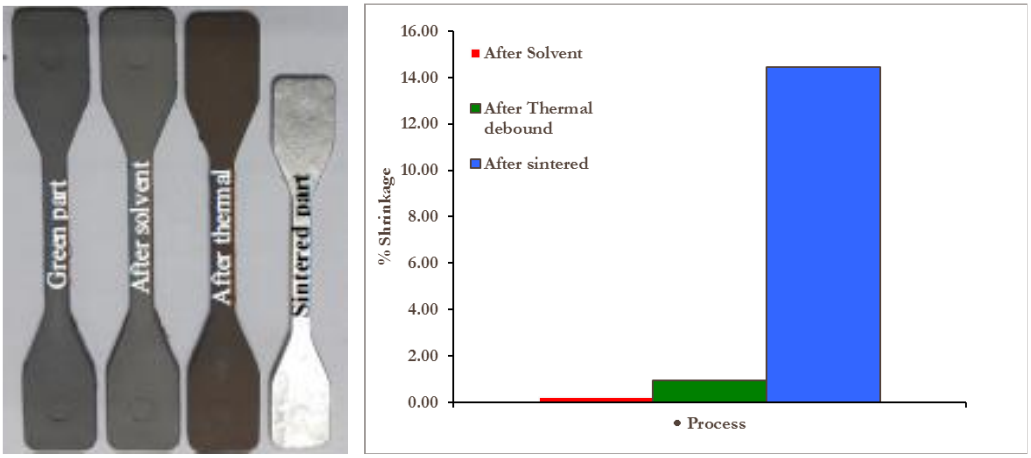

Figure 13: Shrinkage percentage of the sintered, thermal and solvent samples relative to green samples

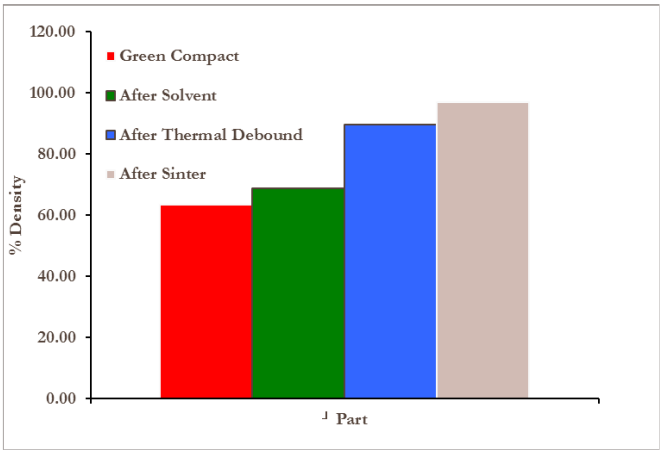

Figure 14: Percentage increase of samples density with respect to pycnometer density of powder after each process

Density of the samples from each processes of the specimens were measured using water immersion method and being compared (Figure 14). After sintering process the samples have higher percentage in density as compare to the green part which is 97%. The density values of the sintered part is 7.8 g/cm3 as compared to thermal and solvent samples which are 7.2 and 5.5 g/cm^3 respectively. This values of density seems acceptable since in powder metallurgy, 97% or higher of density were gain after sintering process and also being compared to other researchers [17].

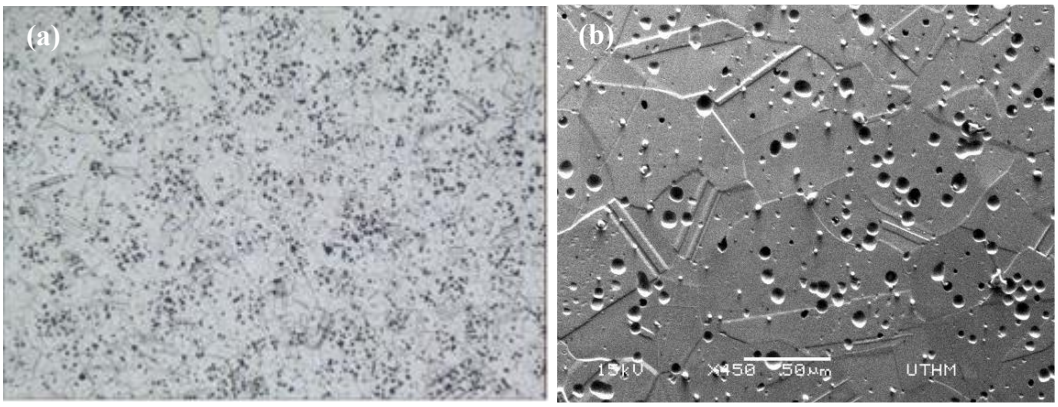

Figure 15: Microstructure of sintered sample a) optical microscope with 100x magnification, b) SEM

Figure 15 shows the microstructure and grains grow of the sintered specimens after etching which indicates typical microstructures of austenitic steel [27]. Pores can be seen on the etched surface of the sintered part. Some pores are still remaining and cannot be eliminated due to isothermal sintering process and these circumstances result in lower sintered density [17]. The tensile strength on the sintered samples was found to be 480MPa with elongation of 14.9 mm. This values seem lower than what have been shown by Omar et. al. [17] due to powder loading used in this experiments was 60% powder loading as compared to 65% powder loading used by Omar et. al. [17]. Higher powder loading will results in higher tensile strength since more powder will reduce the pores inside the samples and reduce the percentage of the part shrinkage besides the effect of heating rates and sintering temperature. Hardness test also being done where the results gain was 250 Hv which is higher than the 200Hv [17].

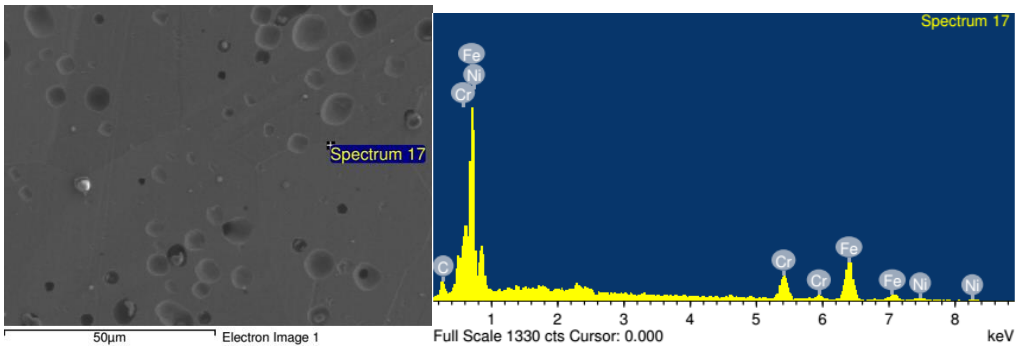

Figure 16: SEM/EDS spot area of the sintered samples

SEM micrograph shows the EDS spot area of the sintered sample (Figure 16) and indicates the passivation area was created on the samples where the present of chromium oxide layer on the surface samples. This passivation layer is important which is functioning as protective oxide layer results in strong resistance of the stainless steel. XRD pattern (Figure 17) of the sintered samples shows the austenite peaks which indicates that after sintering only austenite steel structure exist.

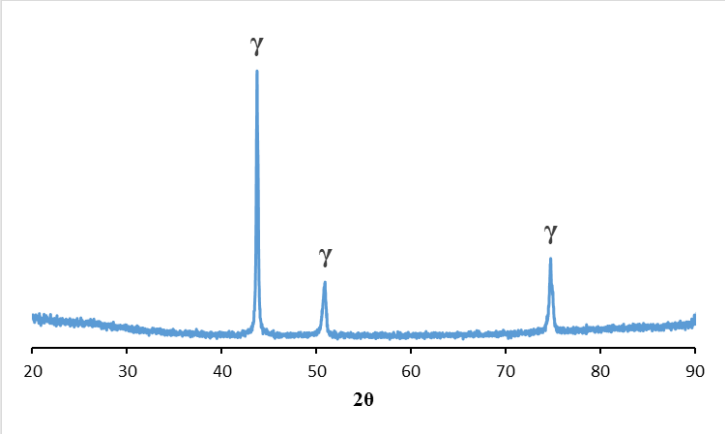

Figure 17: XRD pattern of the sintered sample indicates of γ-austenite peaks

4. Conclusion

From the results and discussion, thermal debinding under all temperature can be used to decompose the PP components of the binder inside the solvent sample without any swelling and cracking. Both samples under 500ºC and 400ºC temperature with heating rate of 10ºC/min of thermal debinding parameters shows decrease in weight components. For 600ºC temperature, percentage of shrinkage was not expected due to the increase in length. Weight of the samples also found to be increases. Samples under 400ºC temperature shows much higher in weight loss due to less oxidation of the samples as compare to the 500ºC samples.

Sintering the samples of 400ºC temperature was successfully done without any distortion. In terms of mechanical properties of the sintered samples, the tensile strength indicates low in value as compare to other researchers which due to lower powder loading used which results in more porosities existence [26]. Microhardness also showing low in value although it is within specification. XRD pattern shows that the formation of γ-austenite steel was developed and β-martensitic structure diminish after the sintering process. This also indicates that the carbon residue from the thermal debinding process was successfully diffuse out of the stainless steel structure.

5. Reference

[1] X. Kong, T. Barriere, and J. C. C. Gelin, "Determination of critical and optimal powder loadings for 316L fine stainless steel feedstocks for micro-powder injection molding," *J. Mater. Process. Technol.*, vol. 212, no. 11, pp. 2173–2182, Nov. 2012.

[2] H. Abolhasani and N. Muhamad, "A new starch-based binder for metal injection molding," *J. Mater. Process. Technol.*, vol. 210, no. 6–7, pp. 961–968, 2010.

[3] S. Ahn *et al.*, "Effect of powders and binders on material properties and molding parameters in iron and stainless steel powder injection molding process," *Powder Technol.*, vol. 193, no. 2, pp. 162–169, Jul. 2009.

[4] M. A. Omar, I. Subuki, N. Abdullah, and M. F. Ismail, "The Influence Of Palm Stearin Content On The Rheological Behaviour Of 316L Stainless Steel MIM Compact," *J. Sci. Technol.*, vol. 2, no. 2, pp. 1–14, 2010.

[5] A. M. Amin, M. H. I. Ibrahim, R. Asmawi, and N. Mustafa, "The Influence of Sewage fat Composition on Rheological Bahavior of Metal Injection Moulding," *Appl. Mech. Mater.*, vol. 660, pp. 38–42, 2014.

[6] L. Liu, N. H. Loh, B. Y. Tay, S. B. Tor, Y. Murakoshi, and R. Maeda, "Effects of thermal debinding on surface roughness in micro powder injection molding," *Mater. Lett.*, vol. 61, no. 3, pp. 809–812, 2007.

[7] M. T. Zaky, "Effect of solvent debinding variables on the shape maintenance of green molded bodies," *J. Mater. Sci.*, vol. 39, no. 10, pp. 3397–3402, 2004.
[8] M. T. Zaky, F. S. Soliman, and A. S. Farag, "Influence of paraffin wax characteristics on the formulation of wax-based binders and their debinding from green molded parts using two comparative techniques," *J. Mater. Process. Technol.*, vol. 209, no. 18–19, pp. 5981–5989, 2009.
[9] G. Aggarwal, S. J. Park, I. Smid, and R. M. German, "Master decomposition curve for binders used in powder injection molding," *Metall. Mater. Trans. A Phys. Metall. Mater. Sci.*, vol. 38, no. 3, pp. 606–614, 2007.
[10] R. K. Enneti, T. S. Shivashankar, S. J. Park, R. M. German, and S. V. Atre, "Master debinding curves for solvent extraction of binders in powder injection molding," *Powder Technol.*, vol. 228, pp. 14–17, 2012.
[11] Y. Tao, Z. Li, and K. Zhou, "Effects of debinding atmosphere on the microstructure and sintering densification of nickel ferrite," *Ceram. Int.*, vol. 39, no. 1, pp. 865–869, 2013.
[12] R. M. German and A. Bose, *Injection Molding of Metals and Ceramics*. Metal powders Industries Federation, 1997.
[13] M. H. . Ibrahim, "Optimization of MicroMetal Injection Moulding Parameter by Design of Experiment Method," Universiti Kebangsaan Malaysia, 2011.
[14] J. M. Adames, "Characterization of Polymeric Binders for Metal Injection Molding (MIM) Process," 2007.
[15] A. M. Amin, M. Halim, I. Ibrahim, R. Asmawi, and N. Mustafa, "Effect of Solvent Debinding Variables on Green Compact With Different Binder Formulation," *ARPN J. Eng. Appl. Sci.*, vol. 11, no. 4, pp. 2442–2447, 2016.
[16] G. J. Shu, K. S. Hwang, and Y. T. Pan, "Improvements in sintered density and dimensional stability of powder injection-molded 316L compacts by adjusting the alloying compositions," *Acta Mater.*, vol. 54, no. 5, pp. 1335–1342, 2006.
[17] M. A. Omar and I. Subuki, "Sintering Characteristics of Injection Moulded 316L Component Using Palm-Based Biopolymer Binder," in *Sintering-Methods and Products*, no. 2012, V. Shatokha, Ed. InTech, 2012, pp. 127–146.
[18] K. A. Khalil, B. Huang, and Y. Li, "Effect of thermo-mechanical properties of PIM feedstock on compacts shape retention during debinding process," *Trans. Nonferrous Met. Soc. China*, vol. 11, no. 4, pp. 521–524, 2001.
[19] Z. Y. Liu, N. H. Loh, S. B. Tor, K. A. Khor, Y. Murakoshi, and R. Maeda, "Binder system for micropowder injection molding," *Mater. Lett.*, vol. 48, no. 1, pp. 31–38, 2001.
[20] K. C. Hsu, C. C. Lin, and G. M. Lo, "The effect of wax composition on the injection molding of carbonyl iron powder with ldpe," *Can. Metall. Q.*, vol. 35, no. 2, pp. 181–187, 1996.
[21] H. M. Shaw and M. J. Edirisinghe, "Shrinkage and particle packing during removal of organic vehicle from ceramic injection mouldings," *J. Eur. Ceram. Soc.*, vol. 15, no. 2, pp. 109–116, 1995.
[22] M. Trunec and J. Cihlář, "Thermal debinding of injection moulded ceramics," *J. Eur. Ceram. Soc.*, vol. 17, no. 2–3, pp. 203–209, 1997.
[23] E. Klar and P. K. Samal, *Powder Metallurgy Stainless Steel-Processing, Microstructure and Properties*, First prin. ASM International The Materials Information Society, 2007.
[24] H. Kotan, "Microstructural evolution of 316L stainless steels with yttrium addition after mechanical milling and heat treatment," *Mater. Sci. Eng. A*, vol. 647, pp. 136–143, 2015.
[25] A. Bautista, F. Velasco, M. Campos, and M. E. Rabanal, "Oxidation Behavior at 900 ° C of Austenitic , Ferritic , and Duplex Stainless Steels Manufactured By Powder Metallurgy," *Oxid. Met.*, vol. 59, no. 30, pp. 373–393, 2003.
[26] A. V. C. Sobral, C. V. Franco, M. P. Hierro, F. J. Pérez, and W. Ristow Jr, "Oxidation of injection molding 316L stainless steel at high temperature," *Mater. Corros.*, vol. 51, no. 11, pp. 791–796, 2000.

[27] M. R. Raza, F. Ahmad, M. A. Omar, and R. M. German, "Effects of cooling rate on mechanical properties and corrosion resistance of vacuum sintered powder injection molded 316L stainless steel," *J. Mater. Process. Technol.*, vol. 212, no. 1, pp. 164–170, 2012.
[28] M. R. Raza, F. Ahmad, M. A. Omar, and R. M. German, "Binder Removal from Powder Injection Molded 316L Stainless Steel," *J. Appl. Sci.*, vol. 11, no. 11, pp. 2042–2047, 2011.